PAPER • OPEN ACCESS

Fermion dark matter and radiative neutrino masses from spontaneous lepton number breaking

New Journal of Physics
The open access journal at the forefront of physics

Deutsche Physikalische Gesellschaft DPG
IOP Institute of Physics

Published in partnership with: Deutsche Physikalische Gesellschaft and the Institute of Physics

OPEN ACCESS

RECEIVED
12 August 2019

REVISED
30 January 2020

ACCEPTED FOR PUBLICATION
3 February 2020

PUBLISHED
6 March 2020

PAPER

Fermion dark matter and radiative neutrino masses from spontaneous lepton number breaking

Cesar Bonilla[1,2,5], **Leon M G de la Vega**[3], **J M Lamprea**[3,4], **Roberto A Lineros**[1] and **Eduardo Peinado**[3]

[1] Departamento de Física, Universidad Católica del Norte, Avenida Angamos 0610, Casilla 1280, Antofagasta, Chile
[2] Physik-Department T30d, Technische Universität München. James-Franck-Strasse, D-85748, Garching, Germany
[3] Instituto de Física, Universidad Nacional Autónoma de México, A.P. 20-364, Ciudad de México 01000, México
[4] Mesoamerican Centre for Theoretical Physics—UNACH, ctra. Zapata km 4, 29040, Tuxtla Gutiérrez, México
[5] Author to whom any correspondence should be addressed.

E-mail: cesar.bonilla@ucn.cl, leonm@estudiantes.fisica.unam.mx, jorge.mario@unach.mx, roberto.lineros@ucn.cl and epeinado@fisica.unam.mx

Keywords: neutrino mass, dark matter, spontaneous lepton number breaking

Abstract

In this paper, we study the viability of having a fermion Dark Matter particle below the TeV mass scale in connection to the neutrino mass generation mechanism. The simplest realisation is achieved within the scotogenic model where neutrino masses are generated at the 1-loop level. Hence, we consider the case where the dark matter particle is the lightest $\mathbb{Z}_2$-odd Majorana fermion running in the neutrino mass loop. We assume that lepton number is broken dynamically due to a lepton number carrier scalar singlet which acquires a non-zero vacuum expectation value. In the present scenario the Dark Matter particles can annihilate via *t*- and *s*-channels. The latter arises from the mixing between the new scalar singlet and the Higgs doublet. We identify three different Dark Matter mass regions below 1 TeV that can account for the right amount of dark matter abundance in agreement with current experimental constraints. We compute the Dark Matter-nucleon spin-independent scattering cross-section and find that the model predicts spin-independent cross-sections 'naturally' dwelling below the current limit on direct detection searches of Dark Matter particles reported by XENON1T.

1. Introduction

The observed fundamental particles as well as their interactions via the strong and electroweak forces are well described under the Standard Model (SM) picture. However, the SM predicts massless neutrinos contradicting neutrino oscillation experiments which indicate that at most one active neutrino can be massless [1–6]. In addition, so far there is no experimental evidence on the exact mechanism chosen by nature to generate neutrino masses. In this regard, the most popular idea to circumvent this mismatch between the SM and neutrino oscillation data is to assume that neutrinos are Majorana particles and invoke the so-called *seesaw* mechanism [7–12]. Furthermore, the SM does not provide a candidate to account for the dark matter (DM) relic abundance in the Universe. The dark matter constitutes about 80% of the matter content of the Universe and its presence is strongly supported by observational evidence at multiple scales, through gravitational effects, its role in structure formation and influence in the features of the Cosmic Microwave Background (CMB). By looking at the CMB and other observables, the Planck collaboration has put the following limit on the dark matter relic abundance [13],

$$\Omega_c h^2 = 0.1200 \pm 0.0012 \quad \text{at} \quad 68\%\ \text{C.L.} \tag{1}$$

Theoretically, it is very tempting to think that the DM sector and neutrino mass generation mechanism are linked. This connection appears naturally when the neutrino masses are generated at the loop level [14]. In such scenarios, the smallness of the neutrino masses is due to a loop suppression and the additional particles carry a non-trivial charge under an unbroken symmetry which is responsible for DM stability. The simplest idea in this regard is the so-called Scotogenic model [14], where the neutrino masses are generated at the 1-loop level. In this

Table 1. Particle content and charge assignments of the model.

	L_i	ℓ_{R_i}	Φ	η	N_i	σ
$SU(2)_L$	2	1	2	2	1	1
$U(1)_Y$	$-1/2$	-1	$1/2$	$1/2$	0	0
$U(1)_L$	-1	-1	0	0	-1	2
$\mathbb{Z}_2$	$+$	$+$	$+$	$-$	$-$	$+$

model, the DM candidate happens to be the lightest particle running inside the loop with an odd charge under a $\mathbb{Z}_2$ discrete symmetry. It could be either bosonic, a CP-even (odd) scalar, or fermionic, a heavy Majorana particle. The strong connection between DM and neutrino mass generation has driven novel studies within this context [15, 16] as well as new variants [17].

Here we have considered the case where the neutrino mass is generated after the spontaneous breaking of lepton number in the Scotogenic model [18] leading to the existence of the Majoron, J, a physical Nambu–Goldstone boson [19, 11]. As a consequence, an invisible Higgs decay channel opens up contributing to its total decay width [20–23]. On top of that, in this model there are two DM annihilation channels when the DM is a Majorana fermion. One is mediated by $\mathbb{Z}_2$-odd particles (t-channel) [24] and the other one (s-channel) [18, 25] coming from the mixing between the scalar singlet and the SM model Higgs after the spontaneous breaking of lepton number and electroweak symmetries. The latter helps to explain DM relic abundance in the Universe for DM masses below the TeV region.

We organized the paper as follows: we introduce the model in the next section. All the constraints used in our analysis are given in section 3. We describe how the analysis is made and we present our results in section 4. Finally, we conclude in section 5.

2. The model

We consider a model where a scalar singlet σ, a $SU(2)_L$ scalar doublet η with hypercharge $1/2$, and three generations of Majorana fermions N_i (with $i = 1, 2, 3$) are added to Standard Model. It is assumed that the scalar doublet $\eta = (\eta^+ , \eta^0)^T$ and the Majorana fermions have an odd charge under an unbroken discrete $\mathbb{Z}_2$ symmetry. This setup can be seen as an extension of the *Scotogenic* model [14]. Hence, the lightest $\mathbb{Z}_2$-odd particle turns out to be a stable DM candidate. Furthermore, we consider the case where the masses of the heavy Majorana fermions are dynamically generated when the scalar singlet gets a vacuum expectation value $\langle\sigma\rangle$. This requires that the scalar singlet σ has a non-trivial charge under lepton number and is responsible of the neutrino mass generation after spontaneous symmetry breaking. The particle content and charge assignments of the model are shown in table 1.

Considering the particle content and additional symmetries, the renormalizable SM $\otimes\, U(1)_L \otimes \mathbb{Z}_2$ invariant Lagrangian for leptons is given by:

$$-\mathcal{L}_Y \supset Y^{\ell}_{ij}\, \bar{L}_i \Phi \ell_{R_j} + Y^{\nu}_{ij}\, \bar{L}_i \tilde{\eta} N_j + \frac{1}{2} Y^{N}_{ij}\, \sigma \bar{N}^c_i N_j + \text{h.c.}, \tag{2}$$

where $\tilde{\eta} = i\tau_2 \eta^*$, $L_i = (\nu_{L_i},\, \ell_{L_i})^T$ with $i, j = e,\, \mu$ and τ. The scalar fields

$$\Phi = \begin{pmatrix} \phi^+ \\ \phi^0 \end{pmatrix} \quad \text{and} \quad \eta = \begin{pmatrix} \eta^+ \\ \eta^0 \end{pmatrix}, \tag{3}$$

denote the usual SM Higgs doublet and the inert doublet respectively. On the other hand, the scalar potential of the model reads

$$\begin{aligned} V = {} & \mu_1^2 \Phi^\dagger \Phi + \mu_2^2 \eta^\dagger \eta + \mu_3^2 \sigma^* \sigma + \lambda_1 (\Phi^\dagger \Phi)^2 + \lambda_2 (\eta^\dagger \eta)^2 + \lambda_3 (\eta^\dagger \eta)(\Phi^\dagger \Phi) \\ & + \lambda_4 (\eta^\dagger \Phi)(\Phi^\dagger \eta) + \frac{\lambda_5}{2} [(\eta^\dagger \Phi)^2 + (\Phi^\dagger \eta)^2] + \lambda_6 (\sigma^* \sigma)^2 \\ & + \lambda_7 (\sigma^* \sigma)(\Phi^\dagger \Phi) + \lambda_8 (\sigma^* \sigma)(\eta^\dagger \eta). \end{aligned} \tag{4}$$

For simplicity, the dimensionless parameters λ_i (with $i = 1, \ldots, 8$) in the last equation are assumed to be real. The scalar singlet σ and the neutral component of the doublet Φ in equation (4) can be shifted as follows

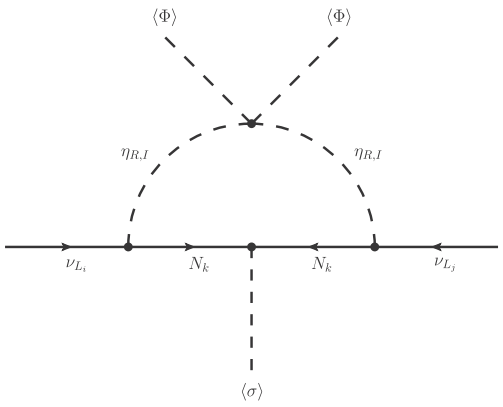

Figure 1. One-loop Feynman diagram for neutrino mass generation.

$$\sigma = \frac{v_\sigma}{\sqrt{2}} + \frac{R_1 + \mathrm{i}\, I_1}{\sqrt{2}} \quad \text{and} \quad \phi^0 = \frac{v_\Phi}{\sqrt{2}} + \frac{R_2 + \mathrm{i}\, I_2}{\sqrt{2}}, \tag{5}$$

where v_a (with $a = \sigma, \Phi$) are the vacuum expectation values and $v_\Phi = 246$ GeV; R_j and I_j (with $j = 1, 2$) represent the CP-even and CP-odd parts of the fields.

2.1. Mass spectrum

Computing the second derivatives of the scalar potential in equation (4) and evaluating them at the minimum of the potential, one gets the CP-even and CP-odd mass matrices, M_R^2 and M_I^2 respectively. There are two CP-odd massless fields, one of them corresponds to the longitudinal component of the Z boson and the other one is a physical Nambu–Goldstone boson resulting from the spontaneous breaking of the $U(1)_L$ symmetry, the Majoron J [19, 11]. Hence,

$$J \equiv I_1, \quad G^0 \equiv I_2. \tag{6}$$

For the CP-even part, one can define the two mass eigenstates h_i through the rotation matrix O_R as follows,

$$\begin{pmatrix} h_1 \\ h_2 \end{pmatrix} = O_R \begin{pmatrix} R_1 \\ R_2 \end{pmatrix} \equiv \begin{pmatrix} \cos\alpha & \sin\alpha \\ -\sin\alpha & \cos\alpha \end{pmatrix} \begin{pmatrix} R_1 \\ R_2 \end{pmatrix}. \tag{7}$$

The angle α is interpreted as the doublet-singlet mixing angle. Then, we have that

$$O_R\, M_R^2\, O_R^T = \mathrm{diag}(m_{h_1}^2,\, m_{h_2}^2), \tag{8}$$

where M_R^2 is the squared CP-even mass matrix whose eigenvalues are given by,

$$m^2_{(h_1,h_2)} = (\lambda_1 v_\Phi^2 + \lambda_6 v_\sigma^2) \mp \sqrt{\lambda_7^2 v_\Phi^2 v_\sigma^2 + (\lambda_1 v_\Phi^2 - \lambda_6 v_\sigma^2)^2}\,, \tag{9}$$

where the '$-$' ('$+$') sign corresponds to h_1 (h_2). Notice that one of these scalar has to be associated to the SM Higgs boson with a 125.09 GeV mass [26]. Furthermore, the masses of the CP-even and CP-odd components of the inert doublet, η, turn out to be

$$m^2_{(\eta_R,\eta_I)} = \mu_2^2 + \frac{\lambda_8}{2} v_\sigma^2 + \frac{\lambda_3 + \lambda_4 \pm \lambda_5}{2} v_\Phi^2. \tag{10}$$

The mass of the charged scalar field is given by,

$$m^2_{\eta^\pm} = \mu_2^2 + \frac{\lambda_3}{2} v_\Phi^2 + \frac{\lambda_8}{2} v_\sigma^2. \tag{11}$$

Notice that the masses of the CP-even and CP-odd fields satisfy the relation $\lambda_5 v_\Phi^2 = (m^2_{\eta_R} - m^2_{\eta_I})$.

As it was mentioned before, neutrino masses are generated dynamically like the rest of the SM fermions. That is, the Majorana masses of N_i as well as the light neutrinos arise after the spontaneous breaking of the global $U(1)_L$ symmetry. From equation (2) follows that the mass matrix for the N_i fields is given by

$$(m_N)_{ij} = \sqrt{2}\, Y^N_{ij}\, v_\sigma. \tag{12}$$

The one-loop neutrino mass generation is depicted in figure 1. After the electroweak symmetry breaking one gets that the light neutrino mass matrix is given by the following expression [14, 18]

$$(M_\nu)_{ij} = \sum_{k=1}^{3} \frac{Y^\nu_{ik}\, Y^\nu_{kj} m_{N_k}}{32\pi^2}\left[\frac{m^2_{\eta_R}}{m^2_{\eta_R} - m^2_{N_k}}\log\frac{m^2_{\eta_R}}{m^2_{N_k}} - \frac{m^2_{\eta_I}}{m^2_{\eta_I} - m^2_{N_k}}\log\frac{m^2_{\eta_I}}{m^2_{N_k}}\right]. \tag{13}$$

3. Summary of constraints

Before analyzing the sensitivities of the experimental searches for WIMPs, we first discuss the theoretical and experimental restrictions that are implemented in our analysis.

3.1. Boundedness conditions

In order to ensure that the theory is perturbative the quartic couplings in the scalar potential, equation (4), as well as the Yukawa couplings in equation (2) are limited to be [27],

$$|\lambda_i|,\ |Y^a_{jk}|^2 \leqslant 4\pi \quad \text{with} \quad i = 1, \ldots, 8;\ j, k = 1, 2, 3 \quad \text{and} \quad a = \nu, \ell, N. \tag{14}$$

Furthermore, the consistency requirements of the scalar potential demand that the dimensionless parameters in equation (4) have to fulfill the following conditions [28],

$$\begin{aligned} &\lambda_1,\ \lambda_2,\ \lambda_6 \geqslant 0, \quad \lambda_3 \geqslant -2\sqrt{\lambda_1\lambda_2}\,, \\ &4\lambda_1\,\lambda_6 \geqslant \lambda_7^2, \quad 4\lambda_2\,\lambda_6 \geqslant \lambda_8^2 \quad \text{and} \quad \lambda_3 + \lambda_4 - |\lambda_5| \geqslant -2\sqrt{\lambda_1\lambda_2}\,. \end{aligned} \tag{15}$$

From the last relations it is guaranteed that the scalar potential is bounded from below.

3.2. Searches of new physics

As we described in the previous section, there are 6 physical scalars in the model: three CP-even $h_i\,(i = 1, 2)$ and η_R; two CP-odd η_I and the Majoron J; and a charged scalar $\eta^\pm$. Therefore, one has to impose the constraints on the scalar masses coming from the LEP results [29] and the latest reports from the LHC on the Higgs properties [30]. Notice that the invisible Higgs decay channel is always present, namely the Higgs decay into Majorons $h \to JJ$, where in our case the SM Higgs h will be identified with either h_1 or h_2. Then, this decay mode coexists with the Higgs decay into the fermion dark matter, N_1, when it is kinematically allowed, i.e. $h \to N_1 N_1$ when $m_{N_1} < m_h/2$. Therefore, we consider [30]

$$\mathcal{B}_{inv} \equiv \text{BR}(h \to \text{invisible}) < 0.28 \quad \text{at} \quad 95\% \quad \text{C.L.} \tag{16}$$

On the other hand, the LEP collaboration studies on the invisible decays of $W^\pm$and Z^0 gauge bosons [29] provide bounds on the masses of the inert scalars $\eta_R(\eta_I)$ and $\eta^\pm$. From these searches, the following conditions must be fulfilled [31]

$$m_{\eta_R} + m_{\eta_I} > m_Z, \quad m_{\eta^\pm} > m_Z/2 \quad \text{and} \quad m_{\eta^\pm} + m_{\eta_{(R,I)}} > m_W. \tag{17}$$

The LEP reports also established disallowed mass regions for the mass splitting given by,

$$m_{\eta_I} - m_{\eta_R} > 8\ \text{GeV} \quad \text{if} \quad m_{\eta_R} < 80\ \text{GeV} \quad \text{and} \quad m_{\eta_I} < 100\ \text{GeV}, \tag{18}$$

and $m_{\eta^\pm} > 80$ GeV.

Finally, it is important to mention that the oblique parameters S, T and U are also sensitive to new physics [32, 33]. Then, it has to be considered that values of these parameters in the model lie within the following regions [30].

$$S = 0.02 \pm 0.10, \quad T = 0.07 \pm 0.12 \quad \text{and} \quad U = 0.0 \pm 0.09. \tag{19}$$

3.3. Dark matter searches

The abundance of DM in the Universe, given in terms of the cosmological abundance parameter, equation (1), provides restrictions on the parameter space of DM models. Furthermore, there exist constraints coming from searches of DM by experiments using (in)direct detection techniques. The direct dark matter detection experiments have set bounds, for DM masses above 6 GeV, on the dark matter-nucleon spin-independent scattering cross section. The most stringent bounds are set by the XENON1T experiment, that is $\sigma_{\text{SI}} \lesssim 4.1 \times 10^{-47}\ \text{cm}^2$ for a DM mass of 30 GeV at 90% C.L. [34]. On the other hand, the astronomical gamma ray observations constrain the velocity averaged cross section of dark matter annihilation into gamma rays $\langle\sigma v\rangle_\gamma$. The Fermi-LAT satellite has performed this indirect DM search and constraint the cross section to be $\langle\sigma v\rangle_\gamma \lesssim 10^{-29}\ \text{cm}^3\ \text{s}^{-1}$ [35]. Notice that there are promising searches using neutrino telescopes like IceCube [36], Antares [37], and KM3Net [38]. Limits on the annihilation cross section for the typical WIMP mass range are not as competitive as other limits obtained with other astroparticle messengers. In additon, neutrinos are

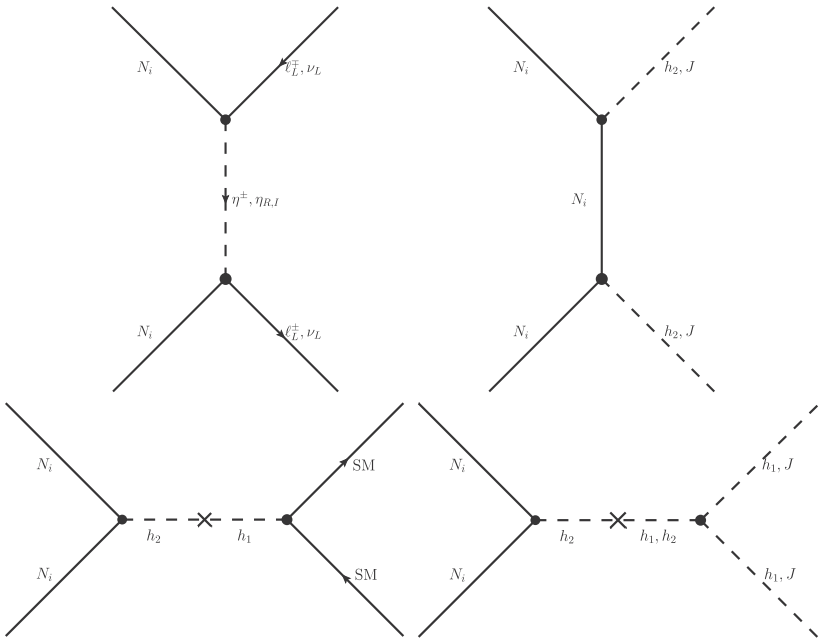

Figure 2. Feynman diagrams for the annihilation channels of the fermion dark matter in the model. On the left annihilation into SM particles. On the right annihilation into Majorons and higgses.

used to set bounds on spin-dependent direct dectection cross section infered from the capture and annihilation of DM in the Sun [39, 40]. The tightest limits are at $m_{\rm DM} \simeq 500$ GeV with $\sigma_{\rm SD} \lesssim 10^{-40}$ cm^2.

3.4. Neutrino oscillation parameters

The neutrino masses are obtained after diagonalisation of the mass matrix given in equation (13). The relation between M_ν and the diagonal mass matrix is given by,

$$M_\nu = U_\nu^* \, \text{diag}(m_{\nu_1}, m_{\nu_2}, m_{\nu_3}) \, U_\nu^\dagger, \tag{20}$$

where m_{ν_i} are the neutrino masses. Here we are not assuming a flavor-diagonal mass matrix for chaged leptons. Therefore, the lepton mixing matrix is difined as $U_L \equiv U_\ell^\dagger U_\nu = U_L(\theta_{12}, \theta_{13}, \theta_{23}, \delta_{\rm CP})$, where θ_{ij} are the mixing angles and $\delta_{\rm CP}$ corresponds to the Dirac CP-violating phase. U_ν and U_ℓ are the matrices that diagonalise the neutrino and charged lepton square mass matrices $M_\nu^\dagger M_\nu$ and $M_\ell M_\ell^\dagger$ respectively. The lepton mixing angles θ_{ij} are determined by neutrino oscillation experiments. From global fits of neutrino oscillation parameters [4] (for other fits of neutrino oscillation parameters we refer the reader to [5, 6]) the best fit values and the 1σ intervals for a normal neutrino mass ordering (NO) are

$$\begin{aligned} &|\Delta m^2_{\rm sol}| = 7.55^{+0.20}_{-0.16} \times 10^{-5}\ \text{eV}^2, \quad |\Delta m^2_{\rm atm}| = 2.50 \pm 0.03 \times 10^{-3}\ \text{eV}^2, \\ &\theta_{12}/^\circ = 34.5^{+1.2}_{-1.0}, \quad \theta_{13}/^\circ = 8.45^{+0.16}_{-0.14}, \quad \theta_{23}/^\circ = 47.7^{+1.2}_{-1.7}, \quad \text{and} \quad \delta_{\rm CP}/^\circ = 218^{+38}_{-27}. \end{aligned} \tag{21}$$

4. Numerical analysis

We have mentioned that the nature of the DM candidate in this model could be either fermionic or scalar. This is the lightest particle with odd charge under the $\mathbb{Z}_2$ symmetry and running in the neutrino mass generation loop as shown in figure 1.

In our study we will focus in the case in which the DM is the lightest Majorana particle[6] , i.e. N_1. Therefore, in this case the DM annihilates via the t- and s-channel in figure 2 . The former is mediated by a Majorana fermion N_i and by the inert scalars. It has been shown that the bounds on lepton flavor violation (LFV) processes, e.g. $\mu \to e\gamma$, demand small neutrino Yukawas (namely, $Y^\nu \ll 1$) and hence the t-channel mediated by the inert scalars becomes suppressed inducing DM overabundance [41, 42]. However, we show that we can keep suppressed the inert scalar mediated t-channel and thanks to the s-channel mediated by the singlet σ it is possible to account for the right amount of DM relic abundance. As a result, it is crucial to have a non-vanishing mixing

[6] In [41–43] has bee analyzed the situation where the DM is the Majorana fermion within the simplest scotogenic model. Note that the case in which the DM is the neutral component of the inert doublet η is similar to the studies for inert doublet model [44].

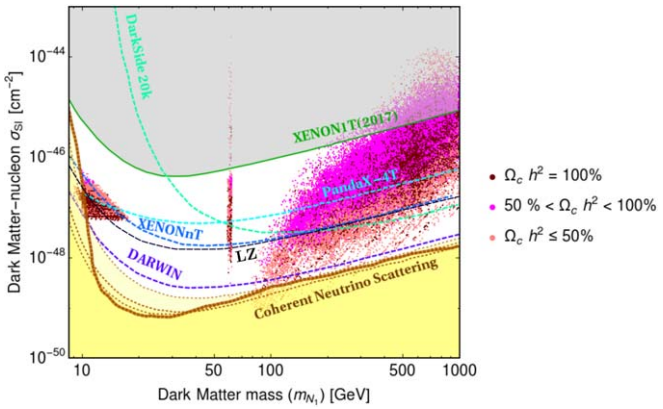

Figure 3. Dark matter mass—σ_{SI} plane showing the solutions in the model that satisfy all theoretical and experimental constraints given in section 3. The latest bound on direct dark matter detection is set by the XENON1T experiment [34] (top shaded area). The dashed lines represent the expected sensitivities in forthcoming experimental searches such as XENONnT [49], LUX-ZEPLIN (LZ) [50], DarkSide 20k [51], DARWIN [52] and PandaX-4T [53].

angle between CP-even parts of the Higgs doublet Φ and the iso-singlet σ, equation (7), and in agreement with current experimental data.

For the numerical analysis we have used the MicrOMEGAS [45] and performed a scan over all free parameters of the model. For the dimensionless parameters in the scalar sector we took the following intervals:

$$10^{-6} \leqslant |\lambda_{2,\ldots,8}| \leqslant 1, \tag{22}$$

and λ_1 being determined by the SM Higgs mass. We are taking h_1 as the SM Higgs then $m_{h_1} = 125$ GeV. On the other hand, we are varying the mass of h_2 within the range $m_{h_2} \in [20,\ 2000]$ GeV. Notice that we are taking masses below 125 GeV which is in perfect agreement with both the LHC and LEP constraints as long as the doublet-singlet mixing given by $\sin\alpha$ in equation (7) is less than 20% [23].

For the masses of the inert scalars we considered the following ranges,

$$m_{\eta_R} \in [110,\ 5000]\ \text{GeV},\quad m_{\eta^\pm} \in [135,\ 5000]\ \text{GeV}, \tag{23}$$

and mass of the CP-odd part η_I is determined by using the relation $\lambda_5 v_\Phi^2 = (m_{\eta_R}^2 - m_{\eta_I}^2)$. For the lepton number breaking scale, namely the singlet's vev v_σ, we have used $v_\sigma \in [500,\ 10000]$ GeV. Bear in mind that this vev provides the mass of the heavy Majorana fermions, N_i, whose masses (taken to be diagonal) are varied in the following ranges,

$$m_{N_1} \in [8,\ 1000]\ \text{GeV}\quad \text{and}\quad m_{N_{2,3}} \in [100,\ 5000]\ \text{GeV}. \tag{24}$$

Since N_1[7] is the DM candidate of the theory we have to impose $m_{N_1} < m_{N_{(2,3)}} < m_{\eta_{(R,I,\pm)}}$[8]. The above considerations are made in such a way that they all satisfy the theoretical and experimental constraints described in section 3. We computed the value of the S and T parameters using the expressions given in [46, 47], taking $U = 0$ [30] and keeping those solutions that are in agreement with the bounds given in equation (19). It is worth to mention that we considered only S and T within the 90% level shown in figure (10.6) from [30]. In addition, we calculated the light neutrino masses feeding the neutrino mass expression given in equation (13) and assumed normal ordering for neutrino masses[9] .Then, we took as valid only the points that satisfy the best fit values from the global fit of neutrino oscillation parameters[10] [4].

Our last requirement is that the annihilation cross section of the fermion DM candidate into Majorons (see figure 2) is subdominant at the moment of the freeze-out in order to guarantee detectability in DM direct detection experiments and to avoid direct detection cross sections in regions far below the neutrino floor.

4.1. Viable dark matter mass regions

Following the considerations that we stated previously, we show in figure 3 the nucleon-dark matter spin-independent cross section σ_{SI} as a function of the fermion DM mass, m_{N_1}. From the numerical analysis we have

[7] There are regions of the parameter space for $M_{N_1} < 8$ GeV but those are below the neutrino floor.

[8] We discard contributions to the DM abundance produced by co-annihilation processes, i.e. $m_{N_{(2,3)}} \lesssim 1.1\ m_{N_1}$.

[9] For simplicity, we have assumed that the Yukawa matrices Y^ν and Y^N are real and diagonal. Following this assumption, the Yukawa matrix for charge lepton is non-diagonal (such that, $U_L = U_\ell^\dagger U_\nu = U_\ell^\dagger$) in order to fit neutrino oscillation experimental data in equation (20).

[10] The sum of neutrino masses was restricted using the cosmological limit provided by Planck, namely $\sum m_\nu < 0.12$eV [48, 13].

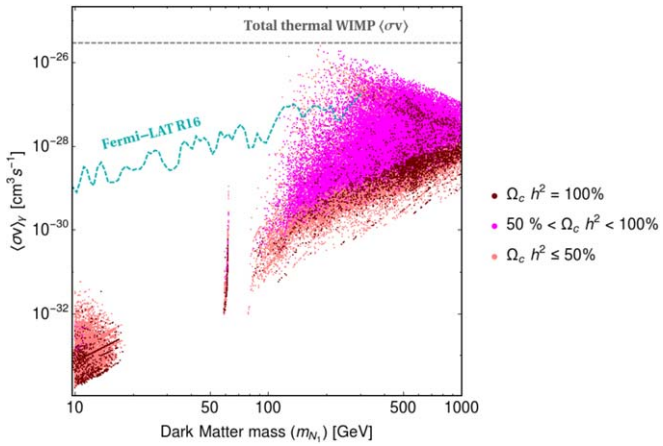

Figure 4. Predictions for the velocity averaged cross section of dark matter annihilation into gamma rays $\langle\sigma v\rangle_\gamma$ as function of the dark matter mass m_{N_1}. The dashed line represent the limit set by Fermi-LAT satellite results [35].

found three different viable mass regions for a fermion DM candidate within the model. We refer as viable to those solutions that fulfill the theoretical and experimental bounds given in section 3. These are:

- *the low mass region*, with an approximate DM mass range 8 GeV $\lesssim m_{N_1} \lesssim$ 20 GeV and $b\bar{b}$ as dominant annihilation channel;
- *the resonant region*, where $m_{N_1} \lesssim m_h/2$ (with $m_h = 125.09$ GeV); and
- *the high mass region*, for DM masses above 80 GeV where the fermion DM annihilates efficiently into the gauge bosons, i.e. $N_1N_1 \to VV$ with $V = (Z, W)$.

In all these domains, the DM annihilation into Majorons ($N_1N_1 \to JJ$) at the moment of the freeze-out is always below 10%. The latest bound coming from direct detection searches of dark matter particles is set the XENON1T experiment [34] and is defined by the top shaded area in figure 3. The dark red points showed in the $m_{N_1} - \sigma_{\rm SI}$ plane account for 100% of the DM relic abundance while the solutions in purple and pink correspond only to a fraction of the DM abundance. Notice that in *the high mass region* it is most likely a fermion DM with a mass around 500 GeV accounting for the whole amount of DM in the Universe. There are few points around $m_{N_1} \sim 10$ GeV and $m_{N_1} \sim 100$ GeV that could not be distinguished from the neutrino floor background (bottom shaded area). Figure 3 also displays the future sensitivities for dark matter searches in direct detection experiments such as XENONnT [49] and LUX-ZEPLIN [50], DarkSide-20k [51], DARWIN [52], and PandaX-4T [53]. For completeness we provide three benchmarks in appendix appendix within each mass neighborhood and their corresponding outputs.

Figure 4 shows the predictions for the velocity averaged cross section of dark matter annihilation into gamma rays $\langle\sigma v\rangle_\gamma$ as function of dark matter mass m_{N_1}. We have found that the annihilation cross section of dark matter into gamma rays is up to two orders magnitude below the limit set by Fermi-LAT satellite results [35] on the indirect DM search (cyan dashed line in figure 4). This is the case for fermion DM with a mass inside the *low mass region*. One can see that there are solutions in the *high mass region* that are ruled out by observations. In particular, the indirect search of DM excludes some points where the fermion DM represent only a fraction of the DM relic abundance. As before, all points satisfy the theoretical and experimental constraints listed in section 3 and the dark red points correspond to the solutions that account for the whole amount of DM in the Universe. The lighter (purple and pink) colors would require the existence of other DM candidates to explain observations, equation (1).

5. Conclusions

In this work we have studied the scotogenic model with spontaneous breaking of lepton number. We have shown that it is possible to account for the whole amount of DM relic density thanks to the scalar singlet used to break lepton number which mixes with the CP-even part of the SM Higgs doublet. Notice that this DM annihilation portal is absent in the simplest version of the scotogenic model, where lepton number is explicitly broken by the Majorana mass term, N_iN_i. In our analysis the LFV processes are suppressed because the neutrino Yukawas are kept small, then experimental constraints are naturally respected. We present a numerical analysis

of the parameter space of the model and the predictions for the nucleon-dark matter spin-independent cross section $\sigma_{\rm SI}$. We show that there are three different DM mass regions that can explain the DM relic abundance, satisfy current experimental constraints as well as the limits on $\sigma_{\rm SI}$ reported XENON1T. We also included the future sensitivities of experiments that are devoted to search for the direct dark matter detection.

Acknowledgments

We would like to thank A Vicente and one of the referees for pointing out a missing factor 1/2 in equation (13). The work of CB was supported by the Collaborative Research Center SFB1258 and UCN Grant 'Neutrino mass generation and BSM' No. 20190803029. RL was supported by Universidad Católica del Norte through the Publication Incentive program No. CPIP20180343. LMGDLV, JML and EP are supported by DGAPA-PAPIIT IN107118 and CONACyT CB-2017-2018/A1-S-13051 (México). CB would like to thank IFUNAM for the hospitality while part of this work was carried out.

Appendix A. Benchmarks

Here we present three benchmarks (BM1, BM2, BM3) corresponding to the different mass regions described in section 4.1 where the fermion DM satisfy all experimental and theoretical constraints summarized in section 3, see tables A1 and A2. Additionally, these representative points are such that the DM particle N_1 constitute 100% of the relic abundance in the Universe, see table A3.

The values for the dimensionless parameters in the Lagrangian as well as the dimensionful parameters in the scalar potential are shown in table A1. Notice that the neutrino Yukawas Y_i^ν (with $i = 1, 2, 3$) are small and as a result LFV processes are suppressed. We include as example in table A2 the branching fractions of $\mu \to e\gamma$ for each benchmark.

Finally, table A3 shows the main DM annihilation channels in the model and prediction in the DM sector.

Table A1. The values for the dimensionful parameters are shown on the top table. The values for the dimensionless parameters in the scalar sector and the neutrino sector are also given.

	m_{N_1}(GeV)	m_{N_2}(GeV)	m_{N_3}(GeV)	m_{η_R}(GeV)	m_{η_I}(GeV)	$m_{\eta^\pm}$ (GeV)	m_{h_2}(GeV)	v_σ (TeV)	μ_2^2 (GeV^2)
BM1	10	119	316	520	536	486	20.7	10.4	2.1×10^5
BM2	59.1	184	410	666	675	645	149	1.08	4.60×10^5
BM3	707	924	940	1132	1119	1119	1498	5.80	6.98×10^6

	$\sin\alpha$	λ_1	λ_2	λ_3	λ_4	λ_5	λ_6	λ_8
BM1	1.31×10^{-1}	1.27×10^{-1}	8.93×10^{-1}	-6.7×10^{-1}	1.4	-2.82×10^{-1}	3.17×10^{-6}	8.19×10^{-4}
BM2	1.57×10^{-1}	1.30×10^{-1}	1	-1.4×10^{-1}	1.1	-1.99×10^{-1}	9.35×10^{-3}	-6.76×10^{-2}
BM3	1.63×10^{-1}	9.23×10^{-1}	1.63	1.63	6.47×10^{-1}	-3.40×10^{-1}	3.24×10^{-2}	-1.48×10^{-1}

	Y_1^N	Y_2^N	Y_3^N	Y_1^ν	Y_2^ν	Y_3^ν
BM1	6.78×10^{-4}	8.04×10^{-3}	2.14×10^{-2}	-1.61×10^{-4}	-4.99×10^{-5}	-4.18×10^{-5}
BM2	3.86×10^{-2}	1.20×10^{-1}	2.68×10^{-1}	-3.22×10^{-5}	-2.75×10^{-5}	-4.70×10^{-5}
BM3	8.61×10^{-2}	1.12×10^{-1}	1.14×10^{-1}	-6.33×10^{-6}	-8.88×10^{-5}	-3.17×10^{-5}

Table A2. The top table shows that (BM1, BM2, BM3) satisfy current experimental constraints in the Higgs sector. The bottom one is used to illustrate how these solutions are in agreement with the bounds coming from LFV processes as well as the electroweak precision tests.

	$\mathcal{B}_{\rm inv}$	BR($h_2 \to JJ$)	BR($h_2 \to h_1 h_1$)	$\Gamma(h_1)$ (MeV)
BM1	3.5×10^{-2}	9.8×10^{-2}	⋯	3.9
BM2	9.7×10^{-2}	9.2×10^{-1}	⋯	4.2
BM3	4×10^{-3}	1.6×10^{-2}	2.3×10^{-1}	3.8

	BR($\mu \to e\gamma$)	S	T
BM1	4.9×10^{-23}	4.3×10^{-3}	3.0×10^{-3}
BM2	6.8×10^{-28}	2.7×10^{-4}	3.2×10^{-3}
BM3	3.8×10^{-28}	6.9×10^{-4}	3.2×10^{-3}

Table A3. Main DM annihilation channels in the model.

	BR ($N_1N_1 \to b\bar{b}$)	BR($N_1N_1 \to JJ$)	BR($N_1N_1 \to h_2h_2$)	BR($N_1N_1 \to ZZ$)
BM1	7.8×10^{-1}	9.8×10^{-2}	⋯	⋯
BM2	5.9×10^{-1}	9.9×10^{-2}	⋯	2.34×10^{-2}
BM3	1.4×10^{-5}	1.4×10^{-2}	⋯	2.37×10^{-1}

	$BR(N_1N_1 \to W^+W^-)$	$\sigma_{\rm SI}$ (pb)	$\langle\sigma v\rangle_\gamma$	$\Omega_c h^2$
BM1	⋯	9.4×10^{-12}	1.7×10^{-34}	1.21×10^{-1}
BM2	2×10^{-1}	3.4×10^{-12}	1.0×10^{-32}	1.20×10^{-1}
BM3	4.7×10^{-1}	2.2×10^{-10}	4.5×10^{-29}	1.19×10^{-1}

ORCID iDs

Cesar Bonilla https://orcid.org/0000-0002-4450-5946

References

[1] Whitehead L H and (MINOS) 2016 *Nucl. Phys.* B **908** 130
[2] Decowski M P and (KamLAND) 2016 *Nucl. Phys.* B **908** 52
[3] Abe K *et al* (T2K) 2017 *Phys. Rev. Lett.* **118** 151801
[4] de Salas P F, Forero D V, Ternes C A, Tortola M and Valle J W F 2018 *Phys. Lett.* B **782** 633
[5] Capozzi F, Lisi E, Marrone A, Montanino D and Palazzo A 2016 *Nucl. Phys.* B **908** 218
[6] Esteban I, Gonzalez-Garcia M C, Hernandez-Cabezudo A, Maltoni M and Schwetz T 2019 *J. High Energy Phys.* **2019** 106
[7] Minkowski P 1977 *Phys. Lett.* B **67** 421
[8] Yanagida T 1979 *Proc.: Workshop on the Unified Theories and the Baryon Number in the Universe, Conf. Proc.* vol C7902131 *(Tsukuba, Japan, 13–14 February 1979)* p 95
[9] Mohapatra R N and Senjanovic G 1980 *Phys. Rev. Lett.* **44** 912
[10] Schechter J and Valle J W F 1980 *Phys. Rev.* D **22** 2227
[11] Schechter J and Valle J W F 1982 *Phys. Rev.* D **25** 774
[12] Foot R, Lew H, He X G and Joshi G C 1989 *Z. Phys.* C **44** 441
[13] Aghanim N *et al* (Planck) 2018 arXiv:1807.06209
[14] Ma E 2006 *Phys. Rev.* D **73** 077301
[15] Hagedorn C, Herrero-García J, Molinaro E and Schmidt M A 2018 *J. High Energy Phys.* **2018** 103
[16] Blennow M, Fernandez-Martinez E, Olivares-Del Campo A, Pascoli S, Rosauro-Alcaraz S and Titov A V 2019 *Eur. Phys. J.* C **79** 555
[17] Fileviez Pérez P, Murgui C and Plascencia A D 2019 *Phys. Rev.* D **100** 035041
[18] Babu K S and Ma E 2008 *Int. J. Mod. Phys.* A **23** 1813
[19] Chikashige Y, Mohapatra R N and Peccei R D 1981 *Phys. Lett.* B **98** 265
[20] Joshipura A S and Rindani S D 1992 *Phys. Rev. Lett.* **69** 3269
[21] Romao J C, de Campos F and Valle J W F 1992 *Phys. Lett.* B **292** 329
[22] Joshipura A S and Valle J W F 1993 *Nucl. Phys.* B **397** 105
[23] Bonilla C, Valle J W F and Romão J C 2015 *Phys. Rev.* D **91** 113015
[24] Kubo J, Ma E and Suematsu D 2006 *Phys. Lett.* B **642** 18
[25] Aranda A, Bonilla C and Peinado E 2019 *Phys. Lett.* B **792** 40
[26] Aad G *et al* (ATLAS, CMS) 2015 *Phys. Rev. Lett.* **114** 191803
[27] Lindner M, Platscher M, Yaguna C E and Merle A 2016 *Phys. Rev.* D **94** 115027
[28] Kadastik M, Kannike K and Raidal M 2009 *Phys. Rev.* D **80** 085020
Kadastik M, Kannike K and Raidal M 2010 *Phys. Rev.* D **81** 029903
[29] Heister A *et al* (ALEPH) 2002 *Phys. Lett.* B **543** 1
[30] Tanabashi M *et al* (Particle Data Group) 2018 *Phys. Rev.* D **98** 030001
[31] Lundstrom E, Gustafsson M and Edsjo J 2009 *Phys. Rev.* D **79** 035013
[32] Peskin M E and Takeuchi T 1990 *Phys. Rev. Lett.* **65** 964
[33] Peskin M E and Takeuchi T 1992 *Phys. Rev.* D **46** 381
[34] Aprile E *et al* (XENON) 2018 *Phys. Rev. Lett.* **121** 111302
[35] Ackermann M *et al* (Fermi-LAT) 2013 *Phys. Rev.* D **88** 082002
[36] Halzen F and Klein S R 2010 *Rev. Sci. Instrum.* **81** 081101
[37] Ageron M *et al* (ANTARES) 2011 *Nucl. Instrum. Methods* A **656** 11
[38] Adrian-Martinez S(KM3Net) *et al* 2016 *J. Phys. G: Nucl. Part. Phys.* **43** 084001
[39] Aartsen M G(IceCube) *et al* 2016 *J. Cosmol. Astropart. Phys.* **2016** 022
[40] Bhattacharya A, Esmaili A, Palomares-Ruiz S and Sarcevic I 2019 *J. Cosmol. Astropart. Phys.* **2019** 051
[41] Toma T and Vicente A 2014 *J. High Energy Phys.* **2014** 160
[42] Vicente A and Yaguna C E 2015 *J. High Energy Phys.* **2015** 114
[43] Ibarra A, Yaguna C E and Zapata O 2016 *Phys. Rev.* D **93** 035012
[44] Belyaev A, Cacciapaglia G, Ivanov I P, Rojas-Abatte F and Thomas M 2018 *Phys. Rev.* D **97** 035011
[45] Belanger G, Boudjema F, Pukhov A and Semenov A 2002 *Comput. Phys. Commun.* **149** 103
[46] Grimus W, Lavoura L, Ogreid O M and Osland P 2008 *J. Phys. G: Nucl. Part. Phys.* **35** 075001
[47] Grimus W, Lavoura L, Ogreid O M and Osland P 2008 *Nucl. Phys.* B **801** 81
[48] Vagnozzi S, Giusarma E, Mena O, Freese K, Gerbino M, Ho S and Lattanzi M 2017 *Phys. Rev.* D **96** 123503
[49] Aprile E(XENON) *et al* 2016 *J. Cosmol. Astropart. Phys.* **2016** 027
[50] Akerib D S(LUX-ZEPLIN) *et al* 2018 arXiv:1802.06039 [astro-ph.IM]
[51] Aalseth C E *et al* 2018 *Eur. Phys. J. Plus* **133** 131
[52] Aalbers J(DARWIN) *et al* 2016 *J. Cosmol. Astropart. Phys.* **2016** 017
[53] Zhang H *et al* (PandaX) 2019 *Sci. China Phys. Mech. Astron.* **62** 31011